Sonic boom reflection over an isolated building and multiple buildings

Didier Dragna, Ariane Emmanuelli, S. Ollivier, Philippe Blanc-Benon

JASA ARTICLE

Sonic boom reflection over an isolated building and multiple buildings

Didier Dragna,[a] Ariane Emmanuelli, Sébastien Ollivier, and Philippe Blanc-Benon
Univ Lyon, Ecole Centrale de Lyon, INSA Lyon, Université Claude Bernard Lyon I, CNRS, Laboratoire de Mécanique des Fluides et d'Acoustique, UMR 5509, 36 Avenue Guy de Collongue, F-69134, Ecully, France

ABSTRACT:
Sonic boom reflection is investigated over an isolated building and multiple buildings using numerical simulations. For that, the two-dimensional Euler equations are solved using high-order finite-difference techniques. Three urban geometries are considered for two boom waves, a classical N-wave and a low-boom wave. First, the variations of the pressure waveforms and the corresponding perceived noise are analyzed along an isolated building. The influence of the building is limited to an illuminated region at its front and a shadow region at its rear, whose size depends on the building's height and the Mach number. Two buildings are then considered. In addition to arrivals related to reflection on the building facades or to diffraction at the building corners, low-frequency oscillations, associated with resonances, are noticed in the street canyon. Their amplitude depends on the street width and on the incident boom frequency contents. Despite their significance, these low-frequency oscillations have little impact on the perceived noise. Finally, a periodic distribution of identical buildings is examined. The duration of the waveforms is notably increased due to multiple diffraction and canyon resonances. Variations in perceived noise at ground level are moderate for large streets, but become noticeable as the street width reduces.
 https://doi.org/10.1121/10.0010452
(Received 15 December 2021; revised 22 April 2022; accepted 24 April 2022; published online 7 June 2022)
[Editor: D. Keith Wilson] Pages: 3792–3806

I. INTRODUCTION

Reducing the boom annoyance generated by supersonic aircraft is a crucial concern for supersonic civil transport. Indeed, civil supersonic flight over land remains banned in the majority of countries due to the sonic boom. The feasibility of low-boom design has been demonstrated for a modified military aircraft (Pawlowski *et al.*, 2005) and the acceptability of low-boom flights by communities should be tested in the next years for a specially designed experimental aircraft (NASA's X-59). If successful, it will be an important step toward lifting the ban and the reappearance of civil supersonic aircraft flying overhead in a longer term. In addition to the development of low-boom concepts, an accurate prediction of the boom signature at the ground and of the corresponding annoyance in realistic configurations is required. The case of urban environments is of major interest.

Moreover, in addition to the exposure outdoors due to the flyover of supersonic aircraft, sonic boom induces an excitation of the buildings. This also leads to annoyance indoors due to the transmitted boom and, predominantly, to rattle noise and structural vibrations [see, among others, Schomer (1978) or Fields (1997)]. To predict these effects, it is necessary to determine the sonic boom signature along the building facade that allows for the evaluation of the dynamic structural loading on the buildings.

Sound propagation in urban environments has been largely investigated in the literature [see, e.g., the handbook by Kang (2007) or the recent review on computational urban acoustics by Hornikx (2016)]. Nevertheless, studies principally deal with road traffic noise, with continuously emitting sources located close to the ground. Sonic boom is specific in that the source is located above the street, as for subsonic aircraft noise, but the signal is of finite duration, with a characteristic wavelength on the order of the supersonic aircraft size.

As indicated in Maglieri *et al.* (2014), sonic boom propagation in an urban environment has been mostly investigated for isolated buildings. Analytical formulations for an incident boom impinging on a two-dimensional (2D) or three-dimensional (3D) rectangular building have been developed in the literature (Ting and Pan, 1968; Ting and Kung, 1972). The different contributions related to the diffraction of the sonic boom at the building corners were discussed. The intensification factor defined as the ratio of the maximal overpressure to that of the incident boom was studied. From geometric considerations, it was shown that it is equal to 4 or 8 for a 2D or 3D 90° corner, respectively, and can be larger for a corner of reduced solid angle.

Experiments at laboratory scale have also been performed. In Brooks *et al.* (1970), the incident sonic boom was generated using a spark source located at the focus of a parabolic mirror. In Bauer and Bagley (1970), the ballistic wave of supersonic projectiles was employed as the small-scale

[a]Electronic mail: didier.dragna@ec-lyon.fr

https://doi.org/10.1121/10.0010452

sonic boom of a supersonic aircraft. Both studies used optical and microphone measurements and investigate sonic boom propagation in the vicinity of an isolated building for several geometries. The measured overpressure waveforms were related to those predicted with the analytical analysis of Ting and colleagues and the intensification factor was determined. Note also that the configuration of two parallel buildings was considered in Bauer and Bagley (1970).

Concerning numerical simulations, standard methods for predicting sonic boom propagation, which are geometrical acoustics and one-way wave equations, are hardly applicable for urban environments. Indeed, geometrical acoustics neglects diffraction, which, in particular, limits its use outside shadow zones, as done by Riegel and Sparrow (2019). Note that geometrical acoustics can be supplemented by analytical edge diffraction models; application of this approach has shown good agreement for an isolated building (Menounou and Nikolaou, 2017; Remillieux *et al.*, 2012), but seems questionable for an urban environment, as multiple diffraction and reflection have to be considered. Besides, one-way wave equations do not account for back-scattering. Resolution of full-wave equations thus appears preferable to deal with sonic boom propagation over urban environments.

Direct numerical simulations are, however, challenging because of the range of length scales involved. Indeed, although the majority of the boom energy is in the low-frequency range, an accurate evaluation of metrics accounting for annoyance requires to solve the high-frequency contents of the boom as well. Therefore, simulations have to be performed on a sufficiently large domain with a size of several sonic boom length but must simultaneously capture the smallest details of the boom wave. The first simulations of sonic boom diffraction by a single building were performed by Cho and Sparrow (2011). The 2D wave equation was solved using finite-difference techniques. The so-called spiking effect was brought to light: the difference in the diffraction of low- and high-frequency contents of the boom wave tends to generate sharp peaks at the shocks. Comparisons with measured booms were also successfully performed. Recently, Yamashita and Nikiforakis (2021) have addressed the problem again. The 2D Euler equations were solved using an adaptive mesh refinement method that aimed at improving grid resolution near the shocks. The evolution of the booms and the perceived noise levels was investigated along the building for different building heights. To the authors' knowledge, no detailed study has been carried out on sonic boom propagation over multiple buildings.

The objective of this paper is to investigate sonic boom propagation over multiple buildings. For this, following the recent study of Emmanuelli *et al.* (2021) on topographic effects on sonic boom propagation, numerical simulations based on the Euler equations are performed. Three urban geometries are examined: an isolated building, two parallel buildings, and a periodic distribution of identical buildings.

The paper is organized as follows. The configurations and the methodology are presented in Sec. II. The case of an isolated building is studied in Sec. III. Sonic boom reflection over multiple buildings is considered, as a first step for two buildings in Sec. IV, and then for a periodic distribution of buildings in Sec. V. Finally, concluding remarks are given in Sec. VI.

II. CONFIGURATIONS AND METHODOLOGY

A. Configurations

The reflection of a sonic boom generated by a supersonic aircraft over an urban geometry is studied. In order to focus the analysis on building effects, it is assumed that the atmosphere is homogeneous and at rest with a constant sound speed c_0 and air density ρ_0, set to $c_0 = 340$ m s^{-1}, and $\rho_0 = 1.22$ kg m^{-3}. The supersonic aircraft cruises at a Mach number M, fixed at $M = 1.6$.

Three urban geometries are investigated and are represented in Fig. 1:

C1 The first one corresponds to an isolated building. Its width W_b is set to 20 m and its height H_b ranges between 10 and 40 m.
C2 The second geometry consists of two identical buildings, whose height and width are set to 10 m and 20 m, respectively. They are separated by a street of width W_s between 10 and 30 m.
C3 The third geometry is made of identical, regularly spaced buildings and is an extension of C2.

Note that 2D configurations are considered, as it allows for an affordable computational cost. We therefore assume that the buildings are infinite in length in the direction perpendicular to the plane of the 2D calculations. This ignores the inherent diffraction effects around the side edges for buildings of finite dimension.

In the three configurations, the buildings have a rectangular shape. Their walls and the ground are rigid.

As in Emmanuelli *et al.* (2021), two incident boom waves are considered. The first one is a classical N-wave, with a maximal amplitude of 24 Pa, a rise time of 0.0011 s,

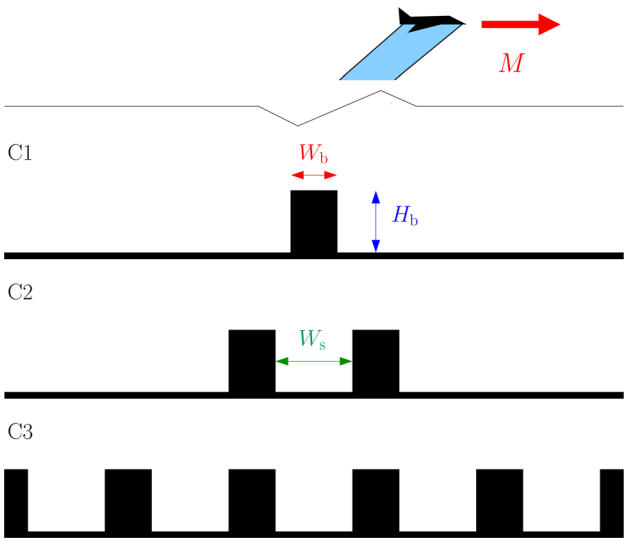

FIG. 1. (Color online) Sketch of the three urban configurations.

and a duration of 0.15 s, corresponding to a characteristic wavelength of 51 m. The N-wave boom has frequency contents up to a few kHz. The second boom wave is a low-boom wave, referred to as the C25D wave. It was obtained by propagating the near-field signature of a notional configuration, used in the 2nd AIAA Sonic Boom Workshop (Rallabhandi and Loubeau, 2019), down to the ground using the BANGV nonlinear ray tracing code (Loubeau and Coulouvrat, 2009). The C25D wave has a maximal amplitude of 20 Pa, a rise time of 0.014 s, and a duration of about 0.1 s. Due to the large rise time, the signal energy of this low-boom wave is contained below 800 Hz.

B. Equations and numerical methods

The 2D Euler equations are solved using high-order finite-difference techniques, developed in the computational aeroacoustics community (Bogey and Bailly, 2004). Simulations are performed using an in-house solver, presented in Emmanuelli *et al.* (2021). This solver was also used to study reflection of weak blast waves above a rough surface in Lechat *et al.* (2021). A moving frame that follows the aircraft trajectory is implemented. It allows for a significant reduction of the number of grid points and hence, of the computational cost. The solver is parallelized using the API OpenMP.

The boundary conditions are similar to those employed in Emmanuelli *et al.* (2021). The sonic boom is injected from the right boundary. On the top boundary, a perfectly matched layer is used as a non-reflecting boundary condition. Along the ground and the walls and roof of the buildings, the normal velocity is set to zero. Finally, as the moving frame is supersonic, the acoustic waves leave the computational domain on its left boundary, without the need of specific treatment.

C. Numerical parameters

The moving frame domain is $L \times H$ with $L = 800$ m and $H = 200$ m. The grid size in the x- and z-directions is the same. It is set to $\Delta x = \Delta z = 0.1$ m for the C25D wave and is reduced to $\Delta x = \Delta z = 0.05$ m for the N-wave. These values are chosen according to the convergence study performed in Emmanuelli *et al.* (2021) and ensure an accurate evaluation of relevant noise metrics. The mesh size of the moving frame is thus 16×10^6 points for the C25D wave and 64×10^6 points for the N-wave.

The moving frame is shifted along the x-direction by a spatial step every two time iterations. The time step and the grid size are then related by $\Delta x = 2Mc_0\Delta t$, in order to make the incident boom stationary in the moving frame. This yields a Courant-Friedrichs-Lewy (CFL) number of $\mathrm{CFL} = c_0\Delta t/\Delta x = 1/(2M)$.

The simulations are carried out using the two-step approach, described in Emmanuelli *et al.* (2021). An initial simulation, denoted by "ini." in Table I, is performed above a flat ground from an initial homogeneous atmosphere. The boom wave then forms progressively from the right boundary. Once the incident boom and the reflected boom on the ground are fully developed, the simulation is stopped. This takes approximately $L/[(M-1)c_0]$, which corresponds to the time for acoustic waves to propagate in the moving frame from the right boundary to the left boundary. The flow variables are then saved and are used for the initialization of the simulations in the urban geometry.

TABLE I. Total simulation time, number of time iterations, and computational time for each configuration simulated.

Configuration		t_{max} (s)	n_t	(CPU hours)
ini.	N	3.7	80 000	8200
	C25D		40 000	900
C1, C2	N	1.8	40 000	2800
	C25D		20 000	300
C3	N	2.8	60 000	4300
	C25D		30 000	500

The total simulation time t_{max} and the number of iterations n_t are indicated for each configuration in Table I. For a given simulation time, the number of time iterations for the N-wave is two times larger than for the C25D wave due to the smaller grid size and the CFL condition.

Simulations are run using 32 core nodes of Intel 6142 Skylake with a clock frequency of 2.6 GHz. An indication of the computational time for the different configurations is provided in Table I. Note that the central processing unit (CPU) time for the initial simulation is longer than that for the simulations of interest with an urban geometry: this shows that the two-step approach allows for a large reduction of CPU time. In addition, the N-wave requires significantly larger computational times than the low-boom wave due to its finer grid.

Two metrics are considered to evaluate sonic boom annoyance. The first one is Stevens' Mark VII perceived level (PL) (Stevens, 1972), which was reported to be the best metric for annoyance evaluation in Leatherwood *et al.* (2002) (although it did not consider sonic boom reflection, which leads to additional peaks and lengthens the waveforms). The second one is the indoor sonic boom annoyance predictor (ISBAP), which was proposed recently (Loubeau *et al.*, 2015) with the aim of predicting indoor annoyance from the outdoor waveform. It is calculated from a linear combination of standard metrics:

$$\mathrm{ISBAP} = \mathrm{PL} + 0.4201(\mathrm{CSEL} - \mathrm{ASEL}), \quad (1)$$

where ASEL and CSEL are the A- and C-weighted sound exposure levels, respectively.

III. ISOLATED BUILDING (C1)

The case of an isolated building is considered first, for two reasons. While it has already been investigated analytically and numerically in the literature, additional information can still be provided by numerical simulations. Moreover, it is used as a baseline for comparison with multiple building configurations.

https://doi.org/10.1121/10.0010452

A. Geometrical analysis

A first insight into the building influence on boom reflection is obtained by a simple geometrical analysis. A sketch is depicted in Fig. 2 showing the rays originating from the incident boom wavefront. Note that the angle of incidence of the plane wavefront is directly related to the Mach number with $\theta = \sin^{-1}(1/M)$. Eight characteristic zones are distinguished. In zones 1, 4, 5, and 8, two rays, corresponding to the incident and reflected rays, reach receivers. The reflected ray originates from the ground in zones 1, 4, and 8 and from the building roof in zone 5. As a consequence, the building is expected to have a negligible effect on the boom in zones 1, 4, and 8. In zone 2, there are three contributions, which are the direct ray, the reflected ray on the ground and an additional contribution due to a ray reflected on the building and on the ground. In zone 3, there are four rays: in addition to the three rays mentioned in zone 2, there is also a ray reflected by the building alone. In zone 7, the only ray reaching a receiver is the direct ray, as the building prevents from any additional contribution. Finally, zone 6 is a shadow zone, with no rays at all.

Along the ground, the building's influence is thus restricted to two regions of same length $H_b \tan\theta = H_b/\sqrt{M^2-1}$: an illuminated region in front of the building in which sound amplification is expected and a shadow zone behind the building. Outside these two regions, the acoustic pressure at the ground is not impacted by the presence of the building with this purely geometric analysis.

B. Acoustic pressure field

Results of the numerical simulations are now considered. Snapshots of the acoustic pressure are depicted at five instants in time in Fig. 3 for the case of an incident N-wave and a building height of $H_b = 10$ m. Note that, as remarked in Emmanuelli *et al.* (2021), the same mechanisms are at play for the two boom waves; maps of acoustic pressure are rather shown for the N-wave than for the C25D wave as the sharp shocks of the N-wave allows for a higher visibility of the wavefronts. The entire evolution of the pressure field is available in Mm. 1 for $H_b =$ 10 m, as well as for $H_b = 40$ m. Despite the simplicity of the configuration, the acoustic pressure field is already notably

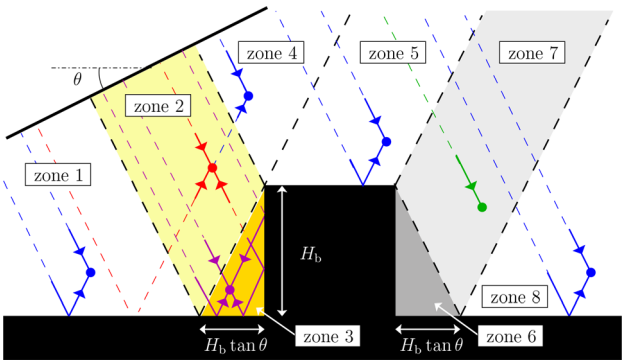

FIG. 2. (Color online) Sketch showing the rays originating from an incident wavefront interacting with a building.

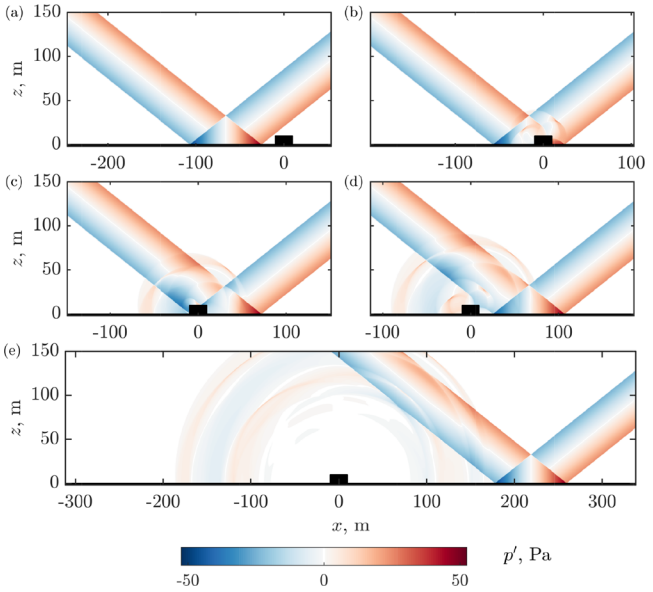

FIG. 3. (Color online) Maps of the acoustic pressure at different instants in time for the case of an incident N-wave impinging on an isolated building of width $W_s = 20$ m and of height $H_b = 10$ m.

complex. It is composed of the incident boom and reflected boom on the ground as well as additional contributions due to reflection on the building front facade and roof and diffraction at the two top building corners. In details, the incident and reflected booms are noticed in (a) and the incident boom impinges on the building. In (b) and (c), the booms are interacting with the building which generates reflected and diffracted waves. In (d), the incident and reflected booms have passed the building and waves generated by the interaction propagate away from the building. Finally, in (e), the incident and reflected booms have recovered their shape with no building and the acoustic pressure in the vicinity of the building is back to zero.

Mm. 1. Video showing the propagation of the N-wave over an isolated building of width $W_b = 20$ m and of height (top) $H_b = 10$ m and (bottom) 40 m.

Additional close-up views of the pressure maps are shown in Fig. 4. Schlieren-like pictures are overlaid on the pressure maps to better distinguish the wavefronts. They are obtained from the modulus of the acoustic pressure gradient $|\nabla p'|$ calculated using finite-difference. The contour lines of $|\nabla p'|$ are then computed and only those whose levels exceed a given threshold, corresponding to strong gradients and therefore to shocks, are plotted using a gray scale. The threshold is the same for all figures (600 Pa m^{-1}), and is chosen to highlight the wavefronts. The front shock of the incident boom is partly reflected on the building roof in (a) and the propagation of the corresponding reflected shock toward the top right of the building is observed in the following views. Similarly, the reflection of the front shock on the front facade is seen in (a). In (b), this reflected shock is again reflected on the ground. Meanwhile, the front shock of

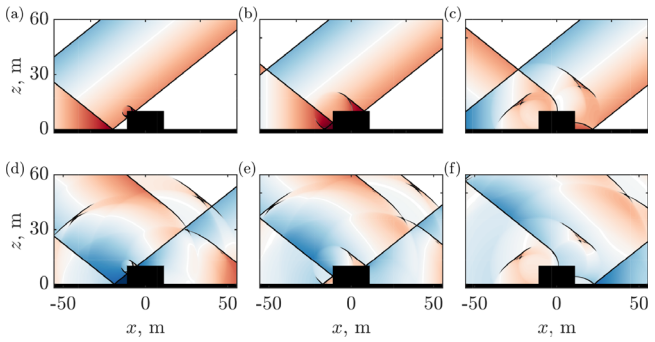

FIG. 4. (Color online) Close-up views of the pressure map showing the diffraction of an N-wave by an isolated building. The colormap is the same as in Fig. 3. Schlieren-like pictures are overlaid to improve shock visualization.

the reflected boom is itself reflected on the front facade. The resulting shock of these two phenomena then propagates toward the top left of the building in (c)–(e). The same pattern is noticed for the rear shock of the incident boom in (d)–(f). Diffraction is also observed, with cylindrical wavefronts generated as shocks are impinging on the top corners of the building.

C. Overpressure waveforms

Overpressure waveforms are shown in Fig. 5 at several locations along the building profile for two building heights ($H_b = 10$ and 40 m) and both for the incident N-wave and C25D wave. They are plotted as a function of the relative time $\tau = t - t_{flat}$, where t_{flat} would be the arrival time of the boom wave on the ground without a building. Note that the length of the illuminated and shadow regions is of 8 m for $H_b = 10$ m and 32 m for $H_b = 40$ m.

At the location at the left of the building ($x = -30$ m) in (a), the signal is composed of several arrivals. The first one at $\tau = 0$ is related to the combination of the incident boom and its reflection on the ground. Note that as the ground is perfectly reflecting, the resulting waveform corresponds to that of the incident boom multiplied by a factor of two. For the N-wave, the shock amplitude is thus close to 50 Pa. The second arrival at $\tau = 0.08$ s is due to the interaction between the incident and reflected booms and the building. For $H_b = 40$ m, this position is located in the illuminated region (zone 3 in Fig. 2): the second arrival is related to reflection on the front facade and has a large amplitude, with a maximum of about 50 Pa for the N-wave. For $H_b = 10$ m, this position is located outside the illuminated region (zone 1 in Fig. 2): the arrival is related to diffraction on the top front corner of the building. It is therefore of reduced amplitude for both boom waves, with a maximum of 12 Pa.

The signal amplitude is maximal at the front bottom corner of the building in (b): the amplitude for the N-wave is thus about 100 Pa, which is four times larger than that of the incident N-wave. In addition, the spiking effect, highlighted by Cho and Sparrow (2011), is observed for $H_b = 10$ m: the front shock presents a sharp peak and a positive peak follows the negative tail shock of the boom. For $H_b = 40$ m, the thickness of the peak on the front shock has notably grown and the amplitude of the peak behind the tail shock has diminished: as already noticed by Cho and Sparrow (2011), the spiking effect is thus largely reduced for sufficiently high buildings and the waveform looks like more an N-wave.

At the front top corner in (c), the incident and reflected booms appear delayed from each other; the delay increases with the building height.

The back top corner is in the shadow zone of the reflected boom. The corresponding signal in (d) is thus composed of the incident boom and then of a second arrival

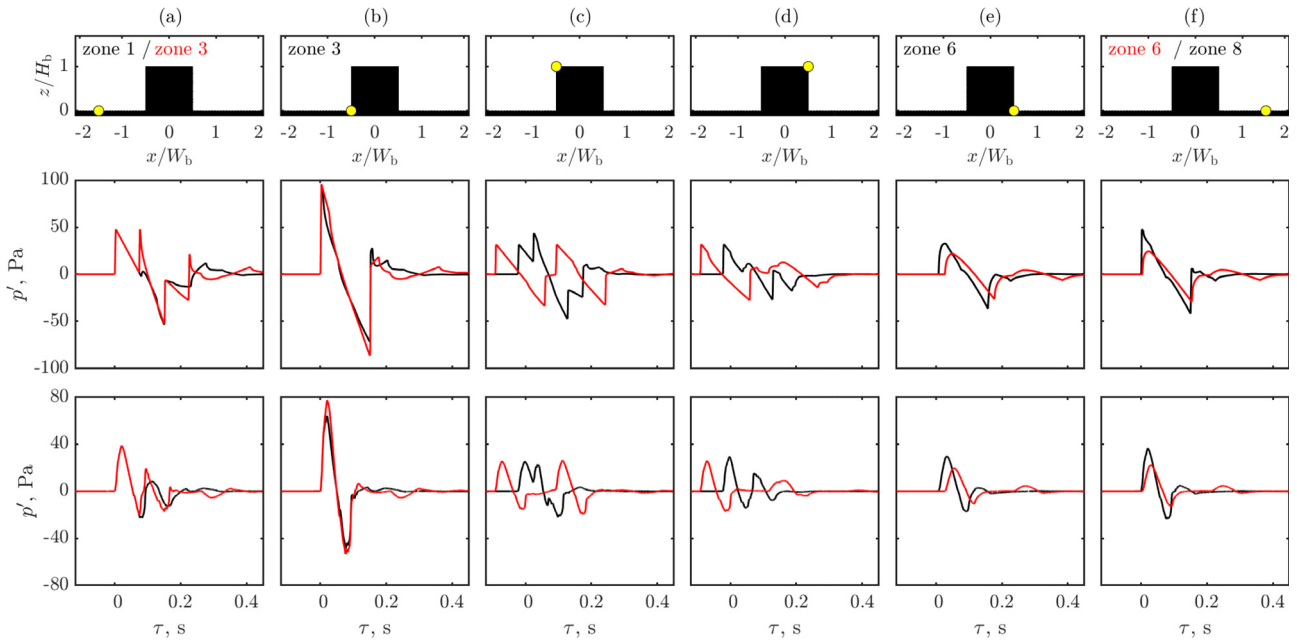

FIG. 5. (Color online) Overpressure waveforms at six different locations along the building profile (middle) for the N-wave and (bottom) for the C25D wave and for two building heights: (black) $H_b = 10$ m and (red) $H_b = 40$ m. Labels for zones correspond to those identified in Fig. 2.

https://doi.org/10.1121/10.0010452

related to the diffraction of the reflected boom on the top front corner. For $H_b = 40$ m, this second arrival at $\tau = 0.12$ s appears rounded compared to the incident wave, because of the larger attenuation of high-frequency contents in the shadow zone.

The back bottom corner in (e) is in the shadow zone for both the incident and reflected booms (zone 6 in Fig. 2). The diffracted waves associated with the incident and reflected booms thus appear rounded.

Finally, (f) shows the overpressure waveforms at a point at the back of the building ($x = 30$ m). For the building height $H_b = 10$ m, the signal has almost recovered its shape in the absence of a building, as the point is located in zone 8 (see Fig. 2), outside the shadow zone. In contrast, for $H_b = 40$ m, the signal is still rounded as the point remains in the shadow zone (zone 6).

D. Noise levels

The perceived noise levels using the metrics PL and ISBAP are computed from the overpressure signals discussed in Sec. III C. They are thereafter normalized by their values on the ground without a building which are 98.2 dB (PL) and 105.9 dB (ISBAP) for the N-wave and 82.8 dB (PL) and 95.3 dB (ISBAP) for the C25D wave to highlight the effect of the building. Note that the PL value for the C25D wave is slightly smaller than that presented in Emmanuelli *et al.* (2021) as an additional low-pass filter has been applied on the waveform to filter out frequency contents above 1 kHz.

Figure 6 shows the map of the perceived noise levels, obtained using the metric PL around an isolated building of height $H_b = 10$ m, for the two boom waves. First of all, due to reflection, the levels are maximal on the wall and decrease rapidly in the direction normal to the wall (about 3 dB in less than one meter). This effect is not clearly observed in Fig. 6 and the evolution of the levels along the walls is discussed subsequently. The boundaries of the geometrical zones presented in Fig. 2 are overlaid in dashed lines. It is noted that the maps are similar for the two boom waves. The maps also correlate well with the geometrical analysis in Sec. III A. In particular in each zone, outside the ground and the building roof and facades, the perceived noise levels are notably homogeneous. In zones 1, 4, 5, and 8, the level is thus equal to −3 dB, while in zone 7, it is about −6 dB, which is the value expected in free-field. In zone 2, the level gradually increases and reaches a value of around −1 dB in the center. Interestingly, there is no large increase in the noise level in the illuminated zone (zone 3). Finally, the shadow zone (zone 6) behind the building is clearly observed and the level reduces as one moves deeper into it.

To further analyze their evolution, the perceived noise levels along the isolated building of height 10 m, including the front and rear facades and the roof, are shown for the N-wave and the C25D wave in Fig. 7. Note that s denotes the position along the building profile. The variations of the levels closely follow the results of the geometrical analysis presented in Sec. III A. Thus, the levels are equal to those obtained without a building, when sufficiently far from it. They progressively increase as one approaches the building. The levels are maximal with a value of +7 dB at the front bottom corner, with corresponding waveform plotted in Fig. 5(b). From geometrical analysis, one can expect the waveform at the corner to be the same as above flat ground, with an amplitude multiplied by two, resulting in a +6 dB increase in noise level. The noise level is thus 1 dB greater than expected. The levels reach a plateau with a value of +4 dB in front of the building and along the front facade, which was referred to as the illuminated zone. Along the roof, they are equal to their values without a building. The levels then decrease sharply in the shadow zone, behind the building. The minimum is at the back bottom corner, with corresponding waveform plotted in Fig. 5(e). It is equal for the N-wave to −14 dB (PL) and −18 dB (ISBAP). It is reminded that 2D simulations are performed and therefore

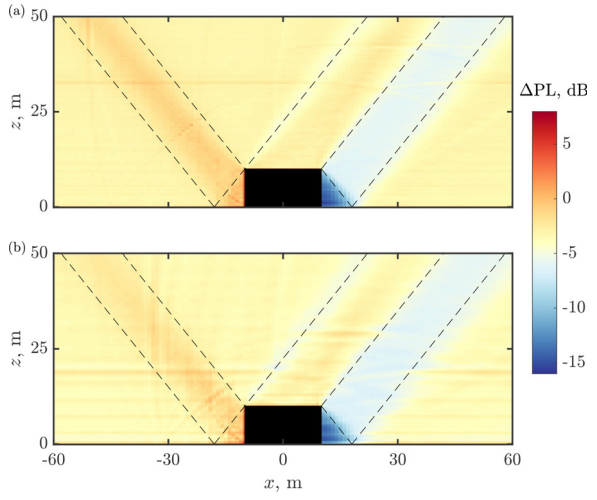

FIG. 6. (Color online) Perceived noise level maps using the metric PL, normalized by its value with no building for: (a) the N-wave and (b) the C25D wave. The building height is $H_b = 10$ m.

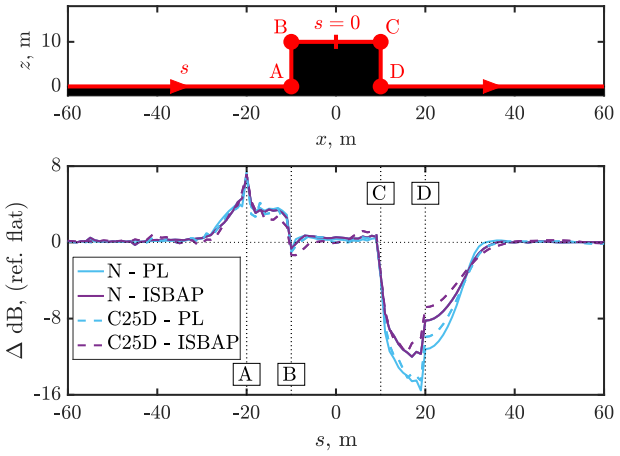

FIG. 7. (Color online) Evolution of the perceived noise levels using the metrics (light blue) PL and (violet) ISBAP along an isolated building of width $W_b = 20$ m and of height $H_b = 10$ m. Results are shown for the N-wave in solid lines and for the C25D wave in dashed lines.

that the building has an infinite length. For a building of finite length, the noise levels inside the shadow zone might be larger because of additional energy brought by diffraction by the side edges. The levels exhibit a jump at the back bottom corner of the building and then progressively increase toward their value without building. Comparing the two metrics, it is noted that the perceived noise levels using either PL or ISBAP metrics show similar variations. Deviations are only observed in the shadow zone where the reduction of levels using the PL metric is greater than that using the ISBAP metric by a few dBs. In addition, the variations of the perceived noise levels relative to the flat ground case are almost the same for the N-wave and the C25D wave.

For comparison, the perceived noise level using the PL metric is plotted along the ground for different building heights in Fig. 8. As indicated above, ISBAP yields analogous results and is not presented for conciseness. The curves for all building heights show close similarities. Especially, the maximum of noise level at the building front corner is about 7 dB for all cases (within 0.3 dB). They differ in the distance they take to increase ahead of the building and to decrease behind it. This length increases with the building height, which is in agreement with the geometrical analysis in Sec. III A, that predicts for a given Mach number a linear increase with the building height of the illuminated region and shadow zone along the ground. Finally, it is found, as discussed in Yamashita and Nikiforakis (2021), that the effect of an isolated building on the noise levels is almost the same, regardless of the incident boom waveform.

IV. TWO BUILDINGS (C2)

This section is devoted to the case of two buildings, as it is the simplest case involving the reflection of booms over multiple buildings.

A. Geometrical analysis

A geometrical analysis is first performed to discuss the conditions, under which interaction between the two buildings can occur. To do so, sound propagation into the street canyon is considered. A sketch is depicted in Fig. 9, showing the trajectory of the incident ray hitting the top of the right building for three street canyon geometries. The key parameter is the aspect ratio of the street canyon AR defined as the ratio of the building height to the street width, i.e., $\mathrm{AR} = H_b/W_s$. For sufficiently large street widths, the rays reflected from the right building do not reach the left building. Thus, there is no interaction between the buildings and it is just as if the buildings were isolated. Interactions occur from $\mathrm{AR}_1 = \sqrt{M^2-1}/2$, for which the ray reflected at the top of the right building's facade hits the top of the left building's facade. As W_s reduces, the interaction should be enhanced; an increase in sound pressure amplitude along the facade of the left building is then expected. A second notable value of the canyon aspect ratio is $\mathrm{AR}_2 = \sqrt{M^2-1}$. For $\mathrm{AR} \geq \mathrm{AR}_2$, the acoustic field on the right building is also expected to be modified compared to an isolated building. First, rays reflected by the left building reach the top of the right building's facade, which should lead to sound amplification. Second, meanwhile, the left building has a shielding effect, preventing the incident rays to reach the facade bottom of the right building, which should lead to sound reduction.

For $M = 1.6$ and for a building height of 10 m, the results are expected to be similar than for an isolated building for street widths larger than 16 m. For W_s between 8 and 16 m, amplification should be observed for the left building, while for $W_s < 8$ m, the acoustic field should also be modified on the right building.

B. Acoustic pressure field

Snapshots of the acoustic pressure field around two buildings with a street width $W_s = 20$ m are shown for the N-wave in Fig. 10 at different instants in time. They are, for the most part, similar to those in Fig. 3 for an isolated building. The main differences can be observed in (e): compared to Fig. 3(e), additional wavefronts propagating away from the buildings are noticed. In addition, while the acoustic pressure in the vicinity of an isolated building was insignificant in Fig. 3(e), some energy is still visible near the two buildings in Fig. 10(e). The evolution of the acoustic field for the N-wave and for the C25D wave is available in Mm. 2.

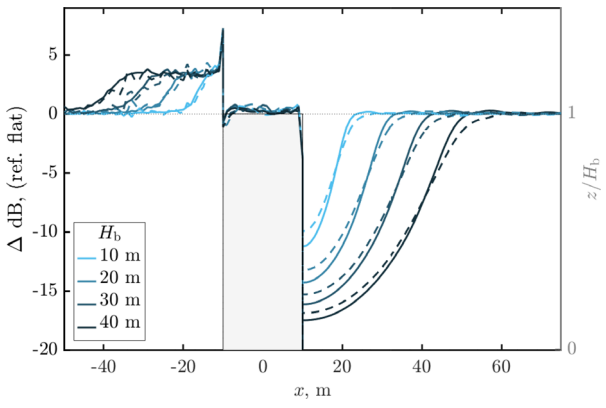

FIG. 8. (Color online) Evolution of the perceived noise levels using the metric PL for the (solid) N-wave and (dash) C25D wave along the ground with an isolated building of width $W_b = 20$ m and of heights H_b between 10 and 40 m.

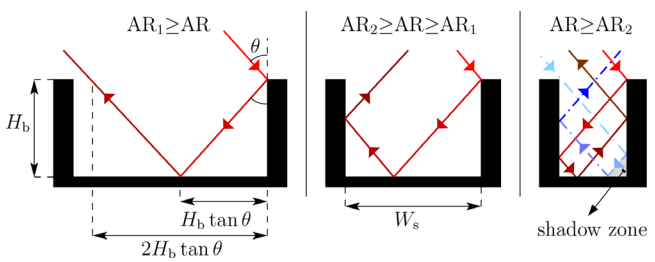

FIG. 9. (Color online) Sketch showing the propagation of rays originating from an incident wavefront inside a street canyon for different canyon aspect ratios.

https://doi.org/10.1121/10.0010452

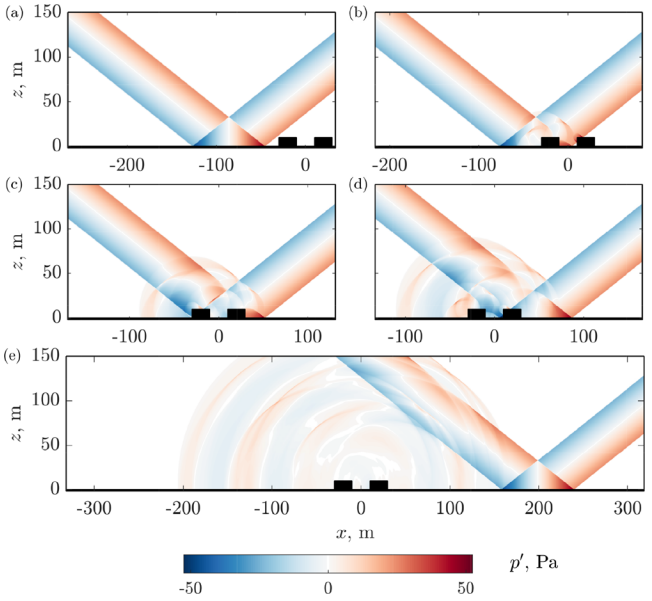

FIG. 10. (Color online) Maps of the acoustic pressure at different instants in time for the case of an incident N-wave impinging on two buildings. The street width is $W_s = 20$ m.

Mm. 2. Video showing the sonic boom propagation over two buildings separated by a street of width $W_s = 20$ m for (top) the N-wave and (bottom) the C25D wave.

In order to characterize the boom propagation inside the street canyon more precisely, close-up views are provided in Fig. 11. They show the wavefront of the incident boom at different instants in time for two street widths of 10 and 20 m. Let us first comment on the pressure maps for $W_s = 10$ m. In (a)–(c), the front shock is diffracted at the top left corner of the street canyon and penetrates into it. The diffracted wave on the corner propagates downwards in (d), is reflected on the street in (e) and then propagates upwards in (f)–(i). In (d), the front shock is reflected on the facade and on the roof of the right building. The wave reflected on the roof reaches that reflected on the roof of the left building in (e) and they propagate rightwards in (f)–(i). The wave reflected on the facade on the right propagates in the canyon in (e), is reflected on the ground in (f), and then propagates upwards in (g). In (h), part of the wave leaves the canyon. The other part is reflected on the facade of the left building, propagates rightwards in (i), and leaves the canyon in (j) while being partly reflected on the right building.

The scenario for $W_s = 20$ m is roughly similar. In particular, the interaction of the incident boom with the right building in (f) still induces a reflected wave impacting the left building in (j). The main difference is that due to the wider street canyon, the reflected wave on the left building does not reflect one more time on the right building. These observations are in agreement with the geometrical analysis done in Sec. III A.

The video showing the propagation of the N-wave inside the street canyon for the three street widths is available in Mm. 3.

Mm. 3. Video showing the propagation of the N-wave in the canyon between the two buildings for street widths (left) $W_s = 10$ m, (middle) 20 m, and (right) 30 m.

C. Overpressure waveforms

The overpressure waveforms obtained at four characteristic points in the street canyon are shown in Fig. 12 for street widths of 10 and 20 m. The corresponding waveforms for the isolated building are also plotted; they can be interpreted as the results for the limiting case $W_s \to \infty$. It is first noted that compared to an isolated building, the signal is much longer. The arrivals for $\tau < 0.2$ s can be identified using geometrical acoustics. Thus, in (a), the first arrival at $\tau = -0.02$ s is the incident boom followed by the reflection of the diffracted wave on the street around $\tau = 0.05$ s. These two arrivals were already present for the isolated buildings. For the N-wave, the third arrival is related to the wave reflected on the right facade. It is seen at $\tau = 0.06$ s with a

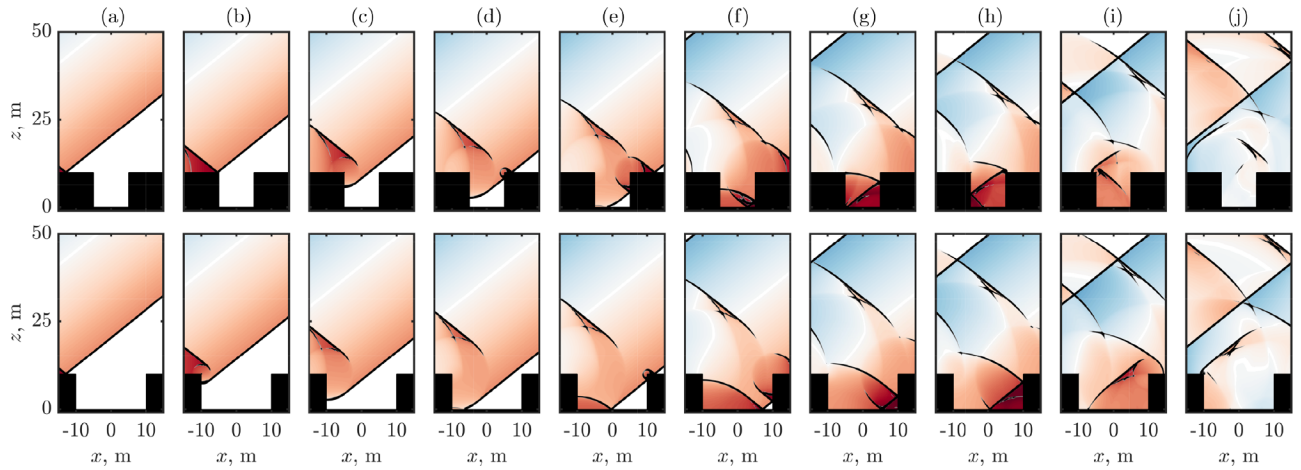

FIG. 11. (Color online) Close-up views showing the propagation of the N-wave front shock inside a street canyon at different instants in time for (top) $W_s = 10$ m and (bottom) $W_s = 20$ m. The colormap is the same as in Fig. 10. Schlieren-like pictures are overlaid to improve shock visualization.

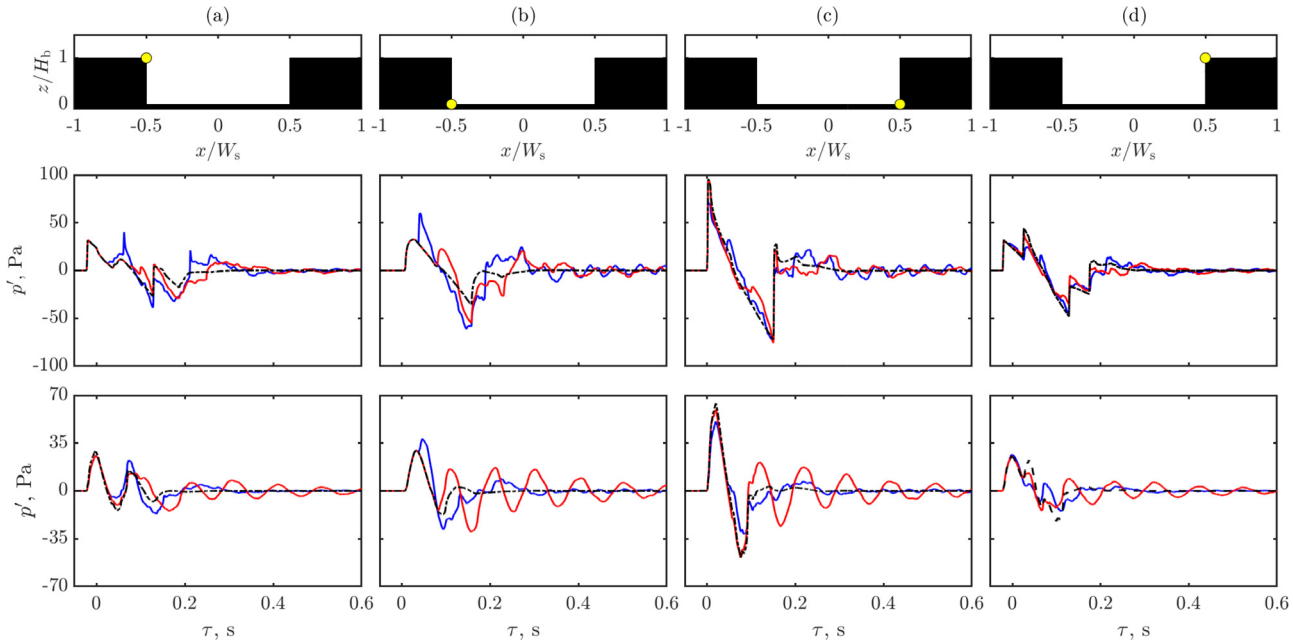

FIG. 12. (Color online) Overpressure waveforms at four different locations in the street canyon between two buildings for (middle) the N-wave and (bottom) the C25D wave and for two street widths: (blue) $W_s = 10$ m and (red) $W_s = 20$ m. For comparison, the waveforms for an isolated building are plotted in a black dashed line.

large amplitude for $W_s = 10$ m and at $\tau = 0.1$ s with a smaller amplitude for $W_s = 20$ m. In (b), in addition to the diffracted wave at the top corner at $\tau = 0$, the reflected wave on the right facade appears at $\tau = 0.04$ s for $W_s = 10$ m and at $\tau = 0.08$ s for $W_s = 20$ m. In (c) and (d), the waveforms look like those for the isolated building. For $W_s = 10$ m, an additional arrival is observed in (d) at $\tau = 0.06$ s that corresponds to the wave that has reflected back and forth in the canyon. At all positions for $\tau > 0.2$ s, the waveforms are composed of low-frequency oscillations that decay slowly with time. This is especially observed for the C25D wave and for $W_s = 20$ m, for which the signal is almost harmonic for $\tau > 0.2$ s: the frequency estimated from the signal is close to 10 Hz. Finally, notice these oscillations have a larger amplitude at the bottom of the canyon than at its top. Note that these low-frequency oscillations can also be distinguished on the overpressure waveforms measured in the canyon between two parallel buildings in the laboratory-scale experiments of Bauer and Bagley (1970).

The effect of the oscillations on the acoustic pressure spectra is now discussed. Figure 13 shows the energy spectral densities (ESDs) of the signal shown in Fig. 12(c) for the N and C25D waves in the low-frequency range. Compared to the ESD for an isolated building, several additional peaks are noticed. These peaks are due to resonant modes of the canyon. Considering the street canyon as an open cavity, the frequency of the modes can be calculated with

$$f_{mn} = \frac{c_0}{2}\sqrt{\left(\frac{m}{W_s}\right)^2 + \left(\frac{1+2n}{2H_b}\right)^2}, \tag{2}$$

where m and n are integers. Note that end correction has not be accounted for. A first broad peak is observed in Fig. 13 at very low frequencies, centered around 4.5 Hz for $W_s = 10$ m, 4 Hz for $W_s = 20$ m, and 3.5 Hz for $W_s = 30$ m. This peak can be related to the first depth mode of the canyon, whose frequency $f_{00} = 8.5$ Hz as given by Eq. (2). A second

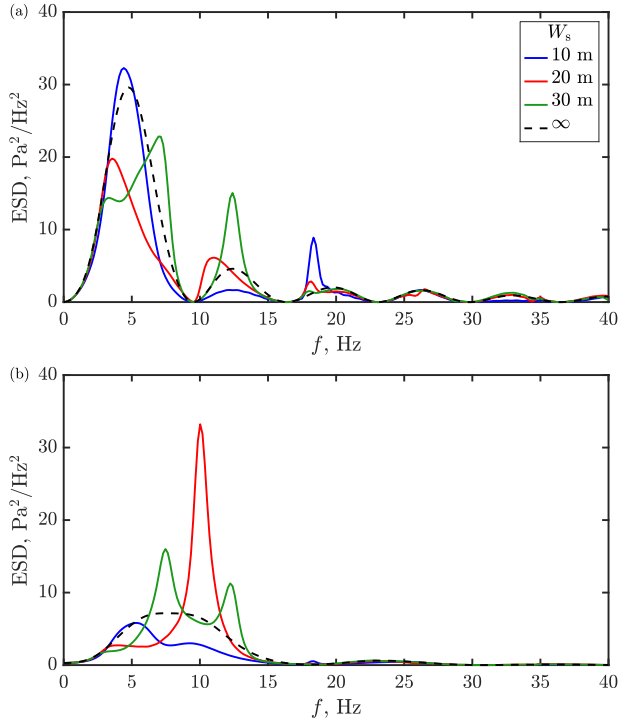

FIG. 13. (Color online) Energy spectral densities of the waveforms in Fig. 12(c) for (a) the N-wave and (b) the C25D wave and for three street widths: (blue) $W_s = 10$ m, (red) $W_s = 20$ m, and (green) $W_s = 30$ m. For comparison, the ESDs for an isolated building are plotted in a black dashed line.

https://doi.org/10.1121/10.0010452

noticeable peak is observed at 18.5 Hz for $W_s = 10$ m, 10 Hz for $W_s = 20$ m, and 7.5 Hz for $W_s = 30$ m. This correlates to the frequency of the first transverse mode in the street canyon f_{10} equal to 19 Hz for $W_s = 10$ m, 12 Hz for $W_s = 20$ m, and 10 Hz for $W_s = 30$ m from Eq. (2). The case $W_s = 20$ m is of particular interest, as it illustrates that the amplitude of the low-frequency oscillations associated with resonant modes of the canyon dramatically depends on the spectrum of the incident boom. For the C25D wave, the peak amplitude at 10 Hz is very large compared to the ESD for one building, which is in agreement with the corresponding waveforms shown in Fig. 12(c). On the contrary, for the N-wave, the ESD at $f = 10$ Hz is almost null, as the frequency of the resonant mode is close to a dip in the N-wave spectrum.

Besides, as 2D simulations are performed, the buildings have an infinite length. This configuration is representative of long streets with continuous buildings. However, if in 3D, there are gaps between the buildings, the effect of canyon resonances might be reduced and the amplitude of oscillations might be smaller.

As a complement, Fig. 14 shows maps of the ESD of the acoustic pressure for three frequencies in the case of an incident C25D wave impinging two buildings with a street width of 10 m. The three frequencies $f = 4.5$, 18.5, and 34.5 Hz have been chosen as they correspond to the frequencies of the peaks of the ESD in Fig. 13. In Fig. 14(a), the pattern inside the canyon is comparable to that of the first depth mode: the ESD is almost uniform in the canyon and decreases outside the canyon. In addition, the ESD in the canyon in Fig. 14(b) shows an evolution corresponding to that of the first transverse mode: the amplitude is maximum on the facades, is zero in the middle of the canyon, and reduces away from the canyon. Finally, the behavior of the ESD in the canyon in Fig. 14(c) is similar to that of the second transverse mode, with a maximum on the facades and

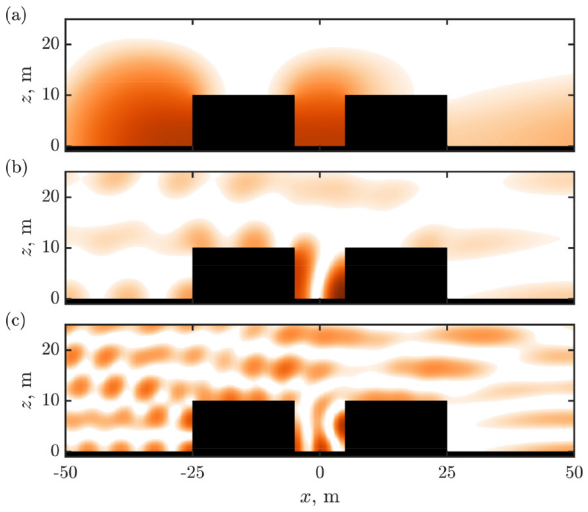

FIG. 14. (Color online) Maps of the energy spectral density of the acoustic pressure for three frequencies: (a) $f = 4.5$ Hz, (b) 18.5 Hz, and (c) 34.5 Hz. Results are shown for an incident C25D wave impinging on two buildings. The street width is $W_s = 10$ m. A logarithmic scale is used and the colour scale ranges over 15 dB, from white to red.

two vertical node lines inside the canyon. This confirms that the peaks observed in Fig. 13 are related to modes of the canyon.

D. Noise levels

The evolution of the perceived noise levels along the urban profile is shown in Fig. 15 for different street widths. For comparison purposes, the case of an isolated building is also plotted in (a). First, note that outside the street canyon, the noise levels at the front of the left building, and at the rear of the right building, are almost equal to those for an isolated building regardless of W_s. In the street canyon for the case $W_s = 30$ m in (b), there is a noticeable increase in noise levels in the shadow zone of the left building: compared to an isolated building, they are amplified by approximately 3.5 dB for the N-wave and 4.5 dB for the C25D wave at the bottom corner of the left building. As one moves away from the left building, the levels increase and recover their values with no building in the middle of the street canyon. The evolution of the noise levels at the front of the right building looks like that of an isolated building. As the street canyon narrows, the levels in the shadow zone of the left building increase. The amplification is modest from $W_s = 30$ m to 20 m, of about 1–2 dB, but is significant for $W_s = 10$ m. In this case, the presence of the buildings leads only to a decrease in about –5 dB (PL) and −3.5 dB (ISBAP) for both boom waves. Finally, for $W_s = 10$ m in (d), the peak of noise levels at the bottom corner of the right building is attenuated with a value of 5 dB, instead of 7 dB; this is due to the shielding effect of the left building.

In addition, it is observed that the low-frequency oscillations observed on the waveforms have little impact on the perceived noise levels. As an example, the signal shown in Fig. 12(c) for the C25D wave and $W_s = 20$ m, presents oscillations of large amplitude; nevertheless, compared to the case of an isolated building, the levels only increase by 0.5 dB (PL) and 0.8 dB (ISBAP). Two factors can explain this result. First, the increase in signal energy remains limited to approximately 1 dB overall. Second, the noise metrics aim at predicting human perception, which tends to reduce significantly the importance of low frequencies. Thus, the evaluation of the PL metric for sonic boom is based on the calculation of loudness. It uses frequency-weighting functions to evaluate the loudness in frequency bands. The total loudness is not directly the sum of the loudnesses in each band, but gives additional weight to the loudest band. Figure 16 illustrates the loudness in third-octave bands for the signals shown in Fig. 12(c). While the signal energy has mostly low-frequency contents (for instance, for C25D and $W_s = 20$ m, more than 95% of the signal energy is below 20 Hz), the loudest bands are between 80 and 400 Hz for the N-wave and between 50 and 200 Hz for the C25D wave. The canyon resonances are found to amplify the loudness at low frequency, especially for the C25D wave, but the low-frequency bands are by far not the loudest and the contribution of the canyon resonances to the total

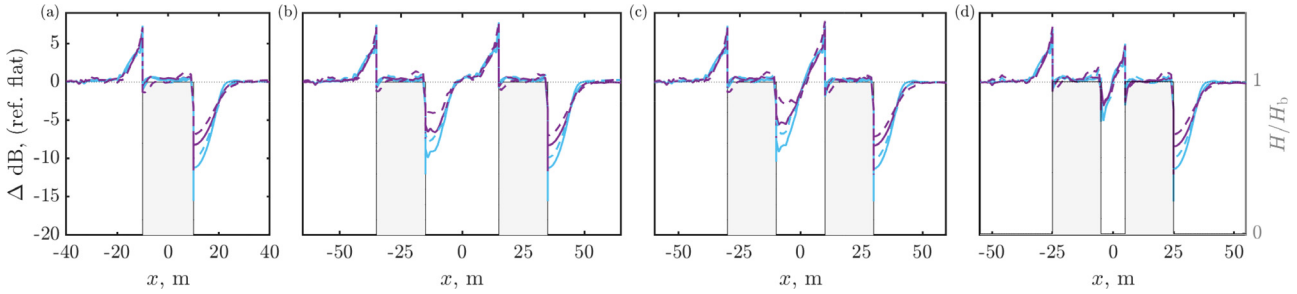

FIG. 15. (Color online) Evolution of the perceived noise levels, using the metrics (light blue) PL and (violet) ISBAP along the ground for (a) an isolated building and two buildings with a street width (b) $W_s = 30$ m, (c) $W_s = 20$ m, and (d) $W_s = 10$ m. Results are shown for the N-wave in solid lines and for the C25D wave in dashed lines.

loudness is marginal. A similar analysis was recently conducted in Yuldashev *et al.* (2021) to study how sonic boom propagation in a turbulent atmosphere impacts the perceived noise level.

V. PERIODIC DISTRIBUTION OF BUILDINGS (C3)

The configuration C3 is now investigated. More specifically, it consists of a distribution of 15 equally spaced, identical buildings with a height of 10 m and a width of 20 m. It was checked that apart from the first two and last five buildings of the profile, the acoustic field is almost independent of the building considered. The results presented in this section correspond to those obtained for the fourth building of the profile.

A. Acoustic field

Figure 17 exemplifies a snapshot of the acoustic pressure for three street widths of 10, 20, and 30 m. The corresponding movie showing the evolution of the acoustic field is available in Mm. 4. While the incident boom is the same, the acoustic field is largely dependent on the street widths. The structure of the reflected boom appears diffuse due to the multiple reflections and diffractions at each building. Above the ground, a series of cylindrical wavefronts propagating toward to the left is observed. Each of these wavefronts is generated every time the incident boom pass over a building of the profile. The distance between two consecutive wavefronts is thus observed to correlate with the street widths.

Mm. 4. Video showing the propagation of the N-wave over a periodic urban profile for street widths (top) $W_s = 10$ m, (middle) 20 m, and (bottom) 30 m.

The pressure waveforms in a street canyon of the periodic urban profile are represented in Fig. 18 for a street width $W_s = 20$ m. For comparison, the waveforms already shown in Fig. 12 for two buildings are also plotted.

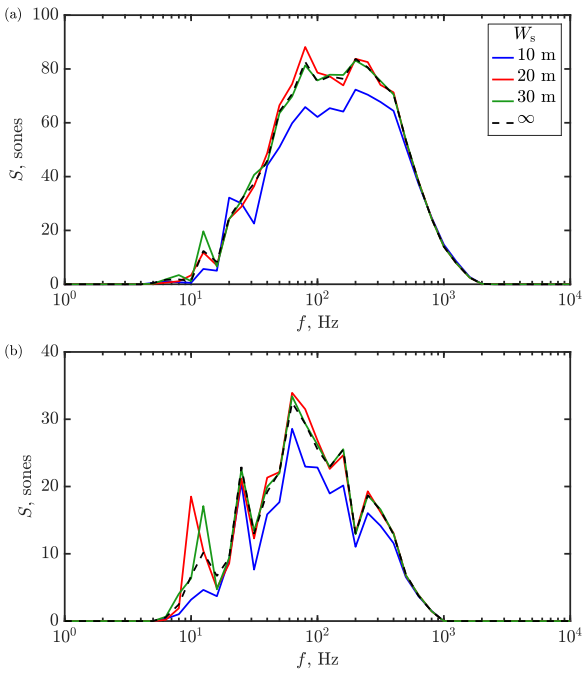

FIG. 16. (Color online) Loudness in third-octave bands computed from the waveforms in Fig. 12(c) for (a) the N-wave and (b) the C25D wave and for three street widths: (blue) $W_s = 10$ m, (red) $W_s = 20$ m, and (green) $W_s = 30$ m. For comparison, the loudness spectra for an isolated building are plotted in a black dashed line.

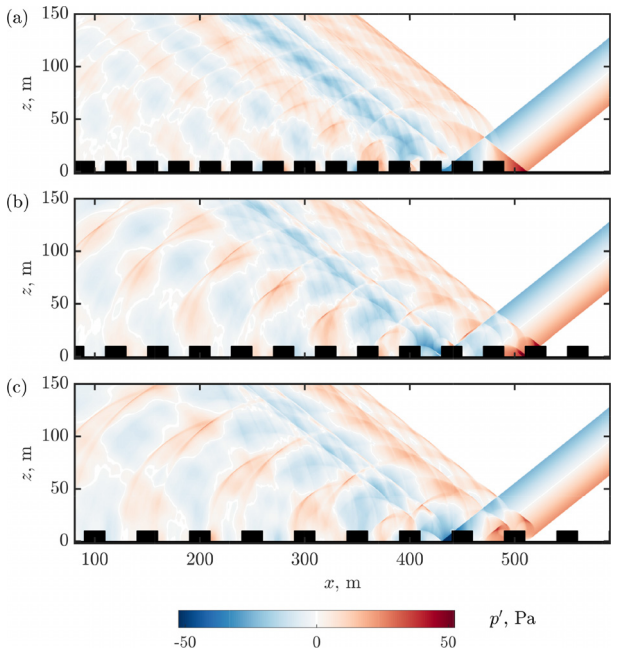

FIG. 17. (Color online) Maps of the acoustic pressure showing an incident N-wave propagating over a regular distribution of identical buildings ($H_b = 10$ m and $W_b = 20$ m) with street widths of (a) 10 m, (b) 20 m, and (c) 30 m.

https://doi.org/10.1121/10.0010452

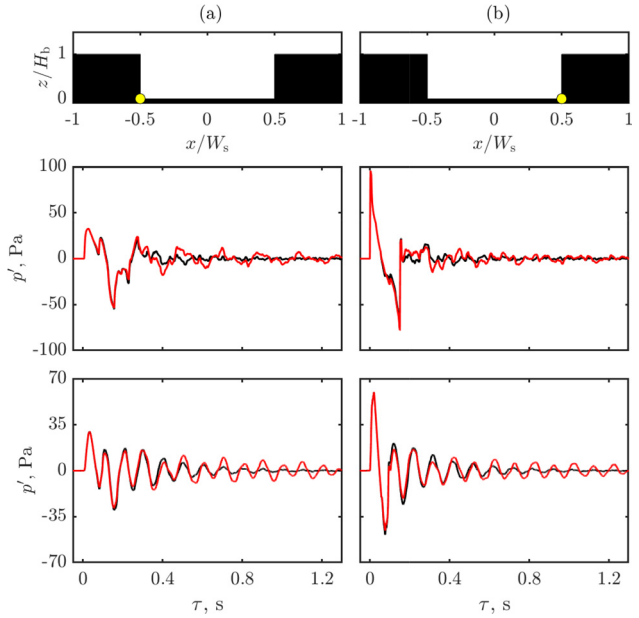

FIG. 18. (Color online) Overpressure waveforms in the street canyon for (middle) the N-wave and (bottom) the C25D in the case of: (black) two buildings and (red) a periodic distribution of identical buildings. The street width is $W_s = 20$ m.

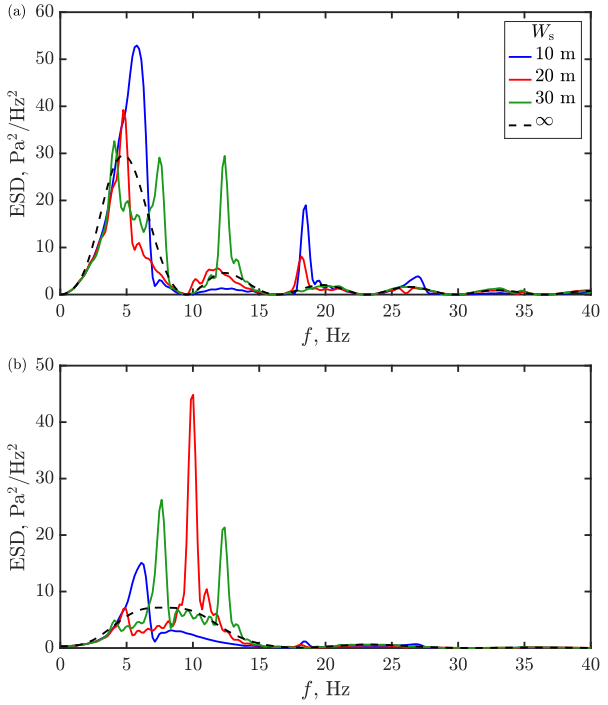

FIG. 19. (Color online) Energy spectral densities of the waveforms in Fig. 18(b) for (a) the N-wave and (b) the C25D wave and for three street widths: (blue) $W_s = 10$ m, (red) $W_s = 20$ m, and (green) $W_s = 30$ m. For comparison, the ESDs for an isolated building are plotted in a black dashed line.

The geometric arrivals for $\tau < 0.2$ s are the same for the two configurations. They are followed by the low-frequency oscillations, discussed in Sec. IV C. These oscillations have a comparable amplitude for the two configurations. However, in the case of a periodic profile, they decrease less rapidly with time; thus, the pressure amplitude remains of a few pascals in the street canyon 1 s after the incident boom has left the canyon.

In order to examine the frequency contents of the oscillations, the energy spectral densities (ESDs) of the signal shown in Fig. 18(b) are plotted in Fig. 19 for the N and C25D waves in the low-frequency range. Two main conclusions can be drawn from this figure. First, comparing with Fig. 13 shows the periodic geometry tends to increase the peak amplitude of the canyon resonance. Second, the periodic distribution of buildings induces the presence of a sharp peak at low frequencies. It is centered at a frequency, slightly above that of the first depth mode, equal to 6 Hz for a street width $W_s = 10$ m, 5 Hz for $W_s = 20$ m, and 4 Hz for $W_s = 30$ m. These two effects could be explained by a periodic forcing of the street canyon by backward-propagating diffracted waves. This idea is illustrated in Fig. 20. At $t = 0$, the incident boom leaves the canyon and propagates toward the next canyon. It is diffracted at the right facade of the second canyon at $t_1 = (W_b + W_s)/(Mc_0)$. The backward-propagating diffracted wave reaches the first canyon at $t_2 = t_1 + (W_b + W_s)/c_0$. Meanwhile, the incident boom pursues its propagation over the urban profile. Another diffracted wave is then generated at the third canyon, that brings back energy in the first canyon at $t_3 = 2t_2$, and so on. Therefore, the periodic generation of diffracted waves induces a periodic forcing of the canyon at the frequency $f_{bd} = 1/t_2$; this yields

$$f_{bd} = \frac{c_0}{W_s + W_b}\frac{M}{1+M}, \tag{3}$$

which gives a correct prediction of the frequencies at the additional sharp peaks in Fig. 19. Note that a periodic

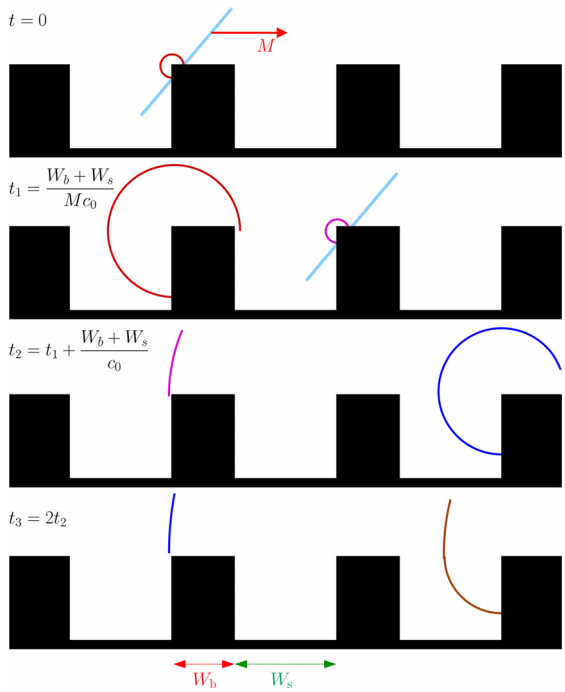

FIG. 20. (Color online) Sketch showing the periodic forcing of the street canyon for a periodic urban profile. See text for details.

forcing is also associated with forward-propagating diffracted waves. A similar reasoning would lead to the forcing frequency:

$$f_{\mathrm{fd}} = \frac{c_0}{W_\mathrm{s} + W_\mathrm{b}} \frac{M}{M-1}. \tag{4}$$

Corresponding peaks are hardly noticeable on the spectra and the forcing by backward-propagating diffracted waves seems to be predominant.

Also, notice that depending on the frequency contents of the incident boom, a particular mode may be dominant. As an illustration, considering Fig. 19 for $W_\mathrm{s} = 30$ m, the mode associated with the periodicity of the urban profile with a forcing frequency of 4 Hz has a larger amplitude for the N-wave, while the mode related to the resonance inside the street canyon with a natural frequency of 7.5 Hz prevails for the C25D wave.

B. Noise levels

The evolution of the perceived noise level using the metric PL normalized by its value for a flat ground is shown along a single building of the periodic profile in Fig. 21, for several street widths. It is plotted from the middle of the street canyon before the building up to middle of the canyon after the building. The results are consistent with those obtained for two buildings in Sec. IV D. Especially, the evolution of the noise level along the building for $W_\mathrm{s} = 30$ m is almost superposed to that for an isolated building: it is equal to its value without building in the middle of the canyon, increases in the front of the building, and significantly reduces in the rear of the building. The main modification compared to an isolated building is the reduction of the shadow zone effect on the noise level: the minimum has increased by +4.2 dB for the N-wave and by +5.8 dB for the C25D wave. The noise level for $W_\mathrm{s} = 20$ m shows the same variations, with a slight amplification in the shadow zone. The largest variation is observed for $W_\mathrm{s} = 10$ m. In this case, the minimum of noise level behind the building is only of −4.5 dB for the N-wave and −4.2 dB for the C25D wave. In addition, the maximum of noise level in front of the building is also reduced to +5 dB for both waves.

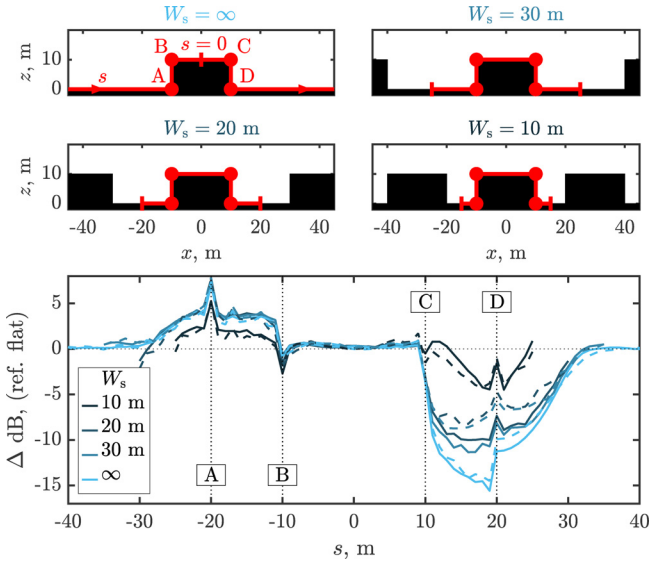

FIG. 21. (Color online) Evolution of the perceived noise levels using the metric PL for (solid) N-wave and (dash) C25D wave along a single building for a periodic distribution of buildings with a width $W_\mathrm{b} = 20$ m and a height $H_\mathrm{b} = 10$ m and for several street widths W_s.

VI. CONCLUSIONS

Sonic boom reflection over an isolated building and multiple buildings was investigated. Numerical simulations based on the 2D Euler equations were performed using high-order finite-difference time-domain techniques. Two boom waves, an N-wave and a low-boom wave, were considered. In the case of an isolated building, a geometrical analysis has highlighted the existence of eight characteristic zones around the building, in particular, an illuminated zone in front of the building and a shadow zone at the back. The spatial evolution of perceived noise levels was shown to be in good accordance with this analysis. Compared to flat ground, the increase in noise levels is of 7 dB at most, at the building corner, and their reduction in the shadow zone depends mostly on the building height. The case of two buildings was then examined. A criterion was deduced from geometrical analysis to predict under which condition interaction between the buildings occurs. For a sufficiently small aspect ratio of the street canyon, the buildings can be considered isolated. As the street width reduces, the acoustic field along the building facades in the street canyon is significantly modified. In particular, low-frequency oscillations were noticed on the pressure waveforms due to canyon resonance, especially with C25D. Its amplitude depends on both the street width and the incident boom wave. Finally, the case of a periodic distribution of identical buildings was considered. The interaction of the incident boom with each building induces a periodic generation of diffracted waves, that bring acoustic energy into the street canyon periodically. This leads to a significant increase in the duration of the acoustic signal, as well as an additional low-frequency peak in the acoustic pressure spectrum. Finally, the noise levels were shown to be slightly modified in the case of multiple buildings with small aspect ratio, compared to an isolated building. As the aspect ratio increases, the levels tend to increase in the shadow zone and to reduce in the illuminated region.

This study yields prospects for future work. First, 2D configurations have been considered. This is an important limitation of the study, as it corresponds to buildings of infinite length in the direction perpendicular to the plane of the 2D calculation. In particular, diffraction around the side edges of the buildings might be important for buildings of finite length and reduce the impact of shadow zones behind isolated buildings, because of the additional energy brought by these diffracted waves. In addition, for multiple buildings, the amplitude of canyon resonances might be reduced if there are gaps between the buildings along the street.

https://doi.org/10.1121/10.0010452

To account for buildings of finite length, 3D simulations should be performed in further work. A second limitation is that sonic boom reflection has only been studied on academic urban profiles; future research must consider more realistic urban profiles. In particular, the statistics of the sonic boom waveforms along the ground will be characterized depending on the geometry of the urban environment. Besides, the geometry of the building was simplified with flat and perfectly reflecting facades; it can be expected that diffusive and absorbing facades will also affect sonic boom reflection.

In addition, the overpressure waveforms on the building facades were found to be dramatically longer for multiple buildings than for an isolated building. Therefore, the duration of the structural loading for multiple buildings will increase accordingly. The metrics are, however, rather unaffected by this effect. Actually, the indoor booms used for the evaluation of metrics in sonic boom simulators are obtained from outdoor booms, either by filtering waveforms using a low-pass filter, which models the building response to the facade excitation (Leatherwood *et al.*, 2002), or by exciting the outer side of an actual representative wall with loudspeaker arrays. The outdoor booms employed are usually synthetized or measured in free-field or above a flat ground and do not account for the urban geometry (and to topography in general) (Naka, 2013; Topken and van de Par, 2021). Besides, it was shown in Sullivan *et al.* (2008) that the duration of the boom signal in simulators needs to be sufficiently long to be perceived as realistic. Thus, it will be interesting to consider more representative outdoor booms, obtained with an urban profile, in order to evaluate the correlation between annoyance and metrics.

ACKNOWLEDGMENTS

This project has received funding from the European Union's Horizon 2020 research and innovation programme under Grant No. N°769896 (RUMBLE). This publication reflects only the author's view and the Innovation and Networks Executive Agency (INEA) is not responsible for any use that may be made of the information it contains. It was performed within the framework of the LABEX CeLyA (ANR-10-LABX-0060) of Université de Lyon, within the program "Investissements d'Avenir" (ANR-16-IDEX-0005) operated by the French National Research Agency (ANR). This work was granted access to the HPC resources of PMCS2I (Pôle de Modélisation et de Calcul en Sciences de l'Ingénieur et de l'Information) of Ecole Centrale de Lyon, PSMN (Pôle Scientifique de Modélisation Numérique) of ENS de Lyon and P2CHPD (Pôle de Calcul Hautes Performances Dédiés) of Université Lyon I, members of FLMSN (Fédération Lyonnaise de Modélisation et Sciences Numériques), partner of EQUIPEX EQUIP@MESO, and IDRIS (Institut du Développement et des Ressources en Informatique Scientifique) under the allocation 2020-02203 made by GENCI (Grand Equipement National de Calcul Intensif).

APPENDIX

Examples of waveforms around an isolated building are presented in this appendix. Figure 22 shows waveforms in the eight zones highlighted in Sec. III A for the N-wave and for a building height of 10 m. The waveforms in zones 1 and 8 are similar: the first contribution around $\tau = 0$ is made of the direct and reflected booms and is followed at $\tau = 0.2$ s

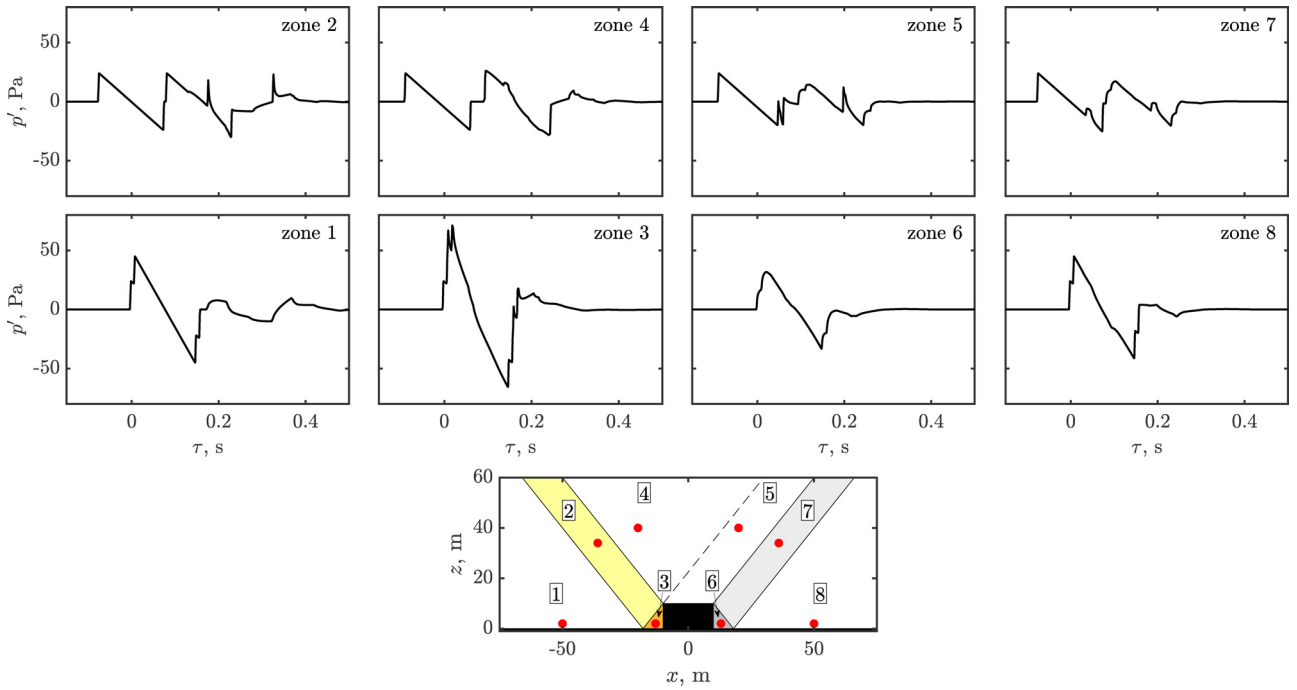

FIG. 22. (Color online) Overpressure waveforms around an isolated building of height $H_b = 10$ m in the eight characteristic zones for the N-wave. The location of each receiver is indicated by a red dot in the sketch at the bottom.

by the boom diffracted by the building. The waveform in the illuminated zone (zone 3) has the largest amplitude. In the shadow zone (zone 6), two contributions associated with the diffracted boom by the building and its reflection on the ground are observed; both show a rounded shock front. Above the building, the waveform in zone 4 is made of the direct boom at $\tau = -0.11$ s and the boom reflected on the ground at $\tau = 0.12$ s. In zone 2, in addition to the direct and reflected booms, two peaks can be noticed at $\tau = 0.18$ s and 0.35 s; they are due to the reflection, on the left facade of the building, of the incident boom and of the reflected boom on the ground. In zone 5, the waveform is slightly more complex. The first contribution at $\tau = -0.09$ s is the direct boom. The two peaks at $\tau = 0.06$ s and 0.2 s are due to the reflection of the boom on the building roof. Their duration is short as the width of the building, $W_b = 20$ m, is small compared to the boom footprint, of approximately 65 m. The last contribution at $\tau = 0.1$ s is due to the diffraction by the building of the reflected boom on the ground; its shock front appears rounded. The waveform in zone 7 is similar to the one in zone 5, except that the two peaks associated with the reflection of the incident boom on the roof have been attenuated.

Bauer, A. B., and Bagley, C. J. (**1970**). "Sonic boom modeling - investigation of topographical and atmospheric effects," FAA-NO-70-10, pp. 1–212.

Bogey, C., and Bailly, C. (**2004**). "A family of low dispersive and low dissipative explicit schemes for flow and noise computations," J. Comput. Phys. **194**, 194–214.

Brooks, J. D., Beasley, W. D., and Barger, R. L. (**1970**). "Laboratory investigation of diffraction and reflection of sonic booms by buildings," NASA TN D-5830, pp. 1–22.

Cho, S.-L. T., and Sparrow, V. W. (**2011**). "Diffraction of sonic booms around buildings resulting in the building spiking effect," J. Acoust. Soc. Am. **129**(3), 1250–1260.

Emmanuelli, A., Dragna, D., Ollivier, S., and Blanc-Benon, P. (**2021**). "Characterization of topographic effects on sonic boom reflection by resolution of the Euler equations," J. Acoust. Soc. Am. **149**(4), 2437–2450.

Fields, J. M. (**1997**). "Reactions of residents to long-term sonic boom noise environments," Contractor Report NASA-CR-201704, NASA, Hampton, VA, pp. 1–167.

Hornikx, M. (**2016**). "Ten questions concerning computational urban acoustics," Build. Environ. **106**, 409–421.

Kang, J. (**2007**). *Urban Sound Environment* (Taylor & Francis, Oxford), Chaps. 4 and 5, pp. 107–174.

Leatherwood, J. D., Sullivan, B. M., Shepherd, K. P., McCurdy, D. A., and Brown, S. A. (**2002**). "Summary of recent NASA studies of human response to sonic booms," J. Acoust. Soc. Am. **111**(1), 586–598.

Lechat, T., Emmanuelli, A., Dragna, D., and Ollivier, S. (**2021**). "Propagation of spherical weak blast waves over rough periodic surfaces," Shock Waves **31**, 379–398.

Loubeau, A., and Coulouvrat, F. (**2009**). "Effects of meteorological variability on sonic boom propagation from hypersonic aircraft," AIAA J. **47**(11), 2632–2641.

Loubeau, A., Naka, Y., Cook, B., Sparrow, V., and Morgenstern, J. (**2015**). "A new evaluation of noise metrics for sonic booms using existing data," AIP Conf. Proc. **1685**, 090015.

Maglieri, D., Bobbitt, P., Plotkin, K., Shepherd, K., Coen, P., and Richwine, D. (**2014**). "Sonic boom: Six decades of research," Technical Report NASA/SP-2014-622, L-20381, NF1676L-18333, NASA, Washington, DC, pp. 1–539.

Menounou, P., and Nikolaou, P. (**2017**). "Analytical model for predicting edge diffraction in the time domain," J. Acoust. Soc. Am. **142**(6), 3580–3592.

Naka, Y. (**2013**). "Subjective evaluation of loudness of sonic booms indoors and outdoors," Acoust. Sci. Tech. **34**(3), 225–228.

NASA. "Low-boom flight demonstration," https://www.nasa.gov/X59/ (Last viewed November 5, 2021).

Pawlowski, J., Graham, D., Boccadoro, C., Coen, P., and Maglieri, D. (**2005**). "Origins and overview of the shaped sonic boom demonstration program," in *43rd AIAA Aerospace Sciences Meeting and Exhibit*, January 10–13, Reno, NV, AIAA-Paper 2005-5, pp. 1–14.

Rallabhandi, S. K., and Loubeau, A. (**2019**). "Summary of propagation cases of the second AIAA sonic boom prediction workshop," J. Aircraft **56**(3), 876–895.

Remillieux, M. C., Corcoran, J. M., Haac, T. R., Burdisso, R. A., and Svensson, U. P. (**2012**). "Experimental and numerical study on the propagation of impulsive sound around buildings," Appl. Acoust. **73**, 1029–1044.

Riegel, K. A., and Sparrow, V. W. (**2019**). "Sonic boom propagation around a large building using a combined ray tracing/radiosity method," J. Acoust. Soc. Am. **145**(4), 2317–2327.

Schomer, P. D. (**1978**). "Human response to house vibrations caused by sonic booms or air blasts," J. Acoust. Soc. Am. **64**(1), 328–330.

Stevens, S. S. (**1972**). "Perceived level of noise by Mark VII and decibels (*E*)," J. Acoust. Soc. Am. **51**(2), 575–601.

Sullivan, B. M., Davies, P., Hodgdon, K. K., Salamone, J. A., and Pilon, A. (**2008**). "Realism assessment of sonic boom simulators," Noise Control Eng. J. **56**(2), 141–157.

Ting, L., and Kung, F. (**1972**). "Diffraction of a plane pulse by a three-dimensional corner," J. Eng. Math. **6**(3), 225–241.

Ting, L., and Pan, Y. S. (**1968**). "Report on sonic boom studies. Part II - Incidence of N-waves on structures," in *Second Conference on Sonic Boom Research*, Washington, DC, May 9-10, NASA SP-180, edited by I. R. Schwartz, pp. 89–98.

Töpken, S., and van de Par, S. (**2021**). "Loudness and short-term annoyance of sonic boom signatures at low level," J. Acoust. Soc. Am. **149**(3), 2004–2015.

Yamashita, R., and Nikiforakis, N. (**2021**). "Numerical simulation of multiple reflections and diffractions of sonic boom around buildings," AIAA J. **59**(7), 2478–2489.

Yuldashev, P. V., Karzova, M. M., Khokhlova, V. A., and Blanc-Benon, P. (**2021**). "Numerical simulation of a nonlinear parabolic equation for analyzing the perceived loudness statistics of sonic boom wave after propagation through atmospheric turbulent layer," Acoust. Phys. **67**(1), 26–37.